Journal of Engineering Mathematics **48:** 353–374, 2004.

A numerical model for the jet flow generated by water impact

D. BATTISTIN and A. IAFRATI
INSEAN - Italian Ship Model Basin - via di Vallerano 139 - 00128 Roma, Italy (e-mails: d.battistin@insean.it; a.iafrati@insean.it)

Received 2 January 2003; accepted in revised form 14 July 2003

Abstract. In this paper a numerical model is developed aimed at describing the jet flow caused by water impact. The study, carried out in the framework of a potential-flow assumption, exploits the shallowness of the jet region to significantly simplify the local representation of the velocity field. This numerical model is incorporated into a fully nonlinear boundary-element solver that describes the flow generated by the water entry of two-dimensional bodies. Attention is focused on the evaluation of the capability of the model to provide accurate free-surface shape and pressure distribution along the wetted part of the body contour, with particular regard to the jet region. After a careful verification, the proposed model is validated through comparisons with the similarity solution of the wedge impact with constant entry velocity. This similarity solution is derived with the help of an iterative procedure which solves the governing boundary-value problem written in self-similar variables.

Key words: jet flow, planing hulls, shallow water, water impact.

1. Introduction

Hydrodynamics loads generated during water impact have a rather evident relevance in terms of structural and dynamic response of ships undergoing slamming. The interest in water impact in the naval field is further supported by the relationship between two-dimensional water entry and hydrodynamics of high-speed craft, as it appears by observing the flow field generated by a planing hull in a earth-fixed imaginary plane orthogonal to the advancing velocity.

Due to the important implications that water impact has in practice, an intense research activity characterised this field since the pioneering works of von Kármán [1] and Wagner [2]. In particular, much attention has been devoted to obtaining the similarity solution of the problem concerning the water entry, with constant velocity, of two-dimensional wedges. In [3] this solution is obtained in the form of a rather complicated nonlinear, singular, integral equation in terms of the free-surface slope. Later, the same solution has been derived by Hughes [4] with the help of conformal mapping involving Wagner's function and, very recently, by de Divitiis and de Socio [5] who sought the solution of the problem through a suitable distribution of singularities in a steady potential-flow field. Apart from combined analytical/numerical approaches, accurate and reliable fully nonlinear numerical procedures have been developed aimed at describing the flow field generated during water entry [6].

In spite of the intense research activity, some unresolved issues, requiring deeper investigation, still exist. One of these issues concerns the prediction and the modelling of the flow-separation phenomenon that can occur as a result of geometric properties of the body contour. Even for a constant entry velocity, flow can detach from convex contours or from impacting bodies having hard chines. In the latter case separation point can be easily identified

while, in the former, its position has to be determined too. The problem is further complicated in the presence of gravity effect or of sudden reductions of the entry velocity in time which make flow separation happen earlier.

The occurrence of flow separation has important implications in determining the pressure distribution along the body contour and, hence, the total hydrodynamic load [7]. Furthermore, when exploiting the analogy between the flow generated by two-dimensional water entry and by planing crafts, a correct estimate of the longitudinal position of flow separation point is imperative for an accurate prediction of the hydrodynamic load and of the position of the center of pressure, both having a relevant role in governing the stability properties of the ship.

In the framework of a potential-flow approximation of an incompressible fluid, an approach that handles this rather complicated problem has been proposed by Vorus [8], at least for shapes of the impacting body characterized by hard chine which fixes the separation point. By using simplifying assumptions based on the flatness of the impacting body, Vorus [8] developed a theory that enforces body and free-surface boundary conditions along their projections on the undisturbed water level but retains all the hydrodynamic nonlinearities. The occurrence of flow separation, which is referred as chine-wetted flow, is accounted for by suitable changes in the boundary conditions. This model has been further generalised to planing hulls by Savander [9] and it has been applied to asymmetric planing surfaces by Xu and Troesch [10] where comparisons with experimental data are also presented.

Within the same potential-flow assumptions, a numerical model able to describe the flow generated during water entry in the presence of flow separation has been developed by Zhao *et al.* [7], as an extension of the fully nonlinear boundary-element approach originally proposed in [6]. In the latter paper a suitable model is introduced to cut off the thin jet that is generated by the flow singularity about the intersection between the free surface and the body contour. This model, which replaces the neglected part of the jet by a suitable boundary condition applied at the jet truncation, is based on the fact that the pressure inside the thin jet is rather negligible, in spite of the high computational effort that would be otherwise needed for an accurate description of the flow in this region. In [7], as soon as the jet truncation passes through the separation point, a Kutta condition is enforced, *i.e.*, it is assumed that the fluid leaves the separation point tangentially and with a finite velocity. The model has been successfully applied to the case of body contours with sharp variation in the slope, while in the case of convex contours, where the separation point has to be determined empirically, the separation mechanisms have not been fully understood.

A numerical approach that could naturally deal with flow separation has been developed by Muzaferjia *et al.* [11], within the viscous-flow assumption of an incompressible fluid. In this model the flow field in both air and water is computed with the help of an additional function, transported by the flow, representing the concentration of the fluids. The interface between air and water is then captured as an iso-contour of the concentration function. Since the interface is not explicitly tracked, the occurrence of flow separation does not require special attention but can simply be recognized by the change in the distribution of the concentration function. It is worth remarking that what makes this approach suitable to deal with separated flows is only related to the numerical model used to discretize the governing equations, while viscous effects are essentially unimportant. As a matter of fact, time scales of the impact process are too short and viscosity cannot play a significant role. A major drawback of this approach is the high computational effort needed to provide an accurate solution.

In [12] an unsteady fully nonlinear boundary-element method has been used to evaluate the hydrodynamic loads generated during the water impact of two-dimensional and axisymmetric

bodies. By use of a model similar to that suggested by Zhao and Faltinsen [6], the jet region is cut off from the computational domain. The method has been applied to the impact, with constant entry velocity, of a circular cylinder and of a sphere. Good agreement with experimental data has been found but only until flow separation takes place, due to the convexity of the body contour. Numerically, flow separation is made evident by the occurrence of negative (relative) pressure on a considerable portion of the wetted body contour. As already noted by Greenhow [13] in the case of the water entry of a wedge, justification for this unphysical behavior has to be attributed to the artificial constraint which is implicitly introduced by keeping the flow attached to the body contour. It is worth noting that, since the most part of the jet region is cut off from the computational domain, nothing is known about the pressure field in the truncated part, thus leading to a delayed prediction of separation.

In the present paper an improved numerical model is presented, which can efficiently and accurately describe the flow and the pressure field inside the thin jet layer. The model, developed in the framework of the potential-flow assumptions, exploits the shallowness of the jet region to reduce the complexity of the governing equations. The need for such a simplified model stems from the difficulty that boundary-element approaches have in representing the solution in very thin layers. Note that separation effects are not considered in the present paper but the developed model is believed to be helpful in achieving this aim.

The basic idea of the model is to take a portion of the jet region and to discretize it with small control volumes. Inside each one, the velocity potential is written in the form of a local expansion, the coefficients of which are recovered by enforcing boundary conditions and matching relations between adjacent volumes. For the first control volume matching relations with the bulk of the fluid, where the solution is described by a classical boundary-element approach, are imposed as well. To make the transition between the bulk of the fluid, S_{bulk}, and the modelled jet region, S_{jet}, smoother, a small number of intermediate control volumes are interposed between them. In this intermediate zone, S_{int}, the velocity potential is written as a weighted average between the velocity potential given by the boundary-element representation and that provided by the local expansions.

A careful verification of the model is carried out when varying the governing parameters. Furthermore, for the purpose of validation, the similarity solution characterizing the wedge impact with constant entry velocity is recovered. This similarity solution is obtained by writing the governing equations in terms of self-similar variables and solving the resulting boundary-value problem with the help of an iterative procedure similar to that used in Iafrati and Korobkin [14] to determine the inner solution of the first-order small-time expansion of a floating wedge impact.

2. Description of the numerical model

2.1. Formulation of the impact problem and its numerical modeling

The unsteady free-surface flow generated during the water entry of two-dimensional symmetric bodies on an initially undisturbed water surface is investigated. The liquid domain is assumed to be infinitely deep and unbounded in the horizontal direction. Let x and y denote the horizontal and vertical axes, respectively, and the impacting body be symmetric, so that the study is limited to the right-hand side of the fluid domain ($x \geq 0$). The entry velocity $\boldsymbol{w} = -V\boldsymbol{e}_y$ is kept constant during the impact, $\boldsymbol{e}_y$ being the unit vector directed along the y-axis.

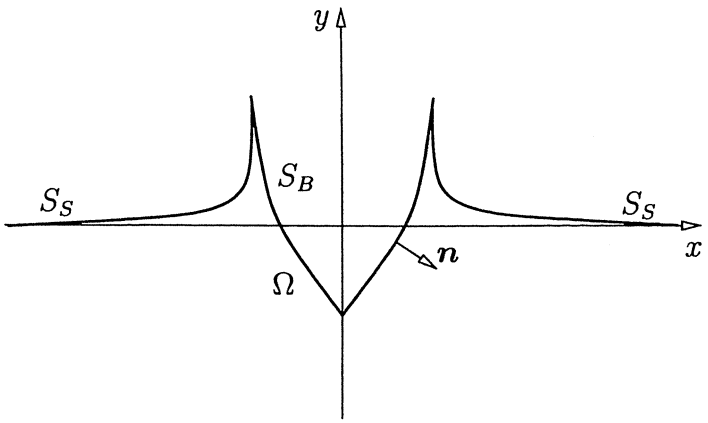

Figure 1. Sketch of the notation adopted. The impact of symmetric bodies is considered.

The study is carried out for an ideal incompressible fluid, with negligible gravity and surface-tension effects. With these assumptions, the flow can be described in terms of a velocity potential φ which satisfies the Laplace equation in the fluid domain Ω, the impermeability constraint on the wetted body contour S_B and the kinematic and dynamic boundary conditions on the free surface S_S, that is

$$\begin{aligned}
&\Delta\varphi = 0 && \text{in} && \Omega,\\
&\varphi_n = -Vn_y && \text{on} && S_B,\\
&\frac{\mathrm{D}\varphi}{\mathrm{D}t} = \frac{|\nabla\varphi|^2}{2} && \text{on} && S_S,\\
&\frac{\mathrm{D}\boldsymbol{x}}{\mathrm{D}t} = \boldsymbol{u} && \text{on} && S_S,
\end{aligned} \tag{1}$$

where $\boldsymbol{n}$ is the unit vector normal to the boundary of the fluid domain oriented inward (Figure 1) and $\mathrm{D}/\mathrm{D}t$ denotes the total derivative. Subscripts on scalar functions denote differentiation with respect to the subscript variable.

The initial-value problem (1) is numerically solved with a mixed Eulerian-Lagrangian approach [15]. At each time step, by using Green's second identity, the solution of the boundary-value problem for φ is sought in the form of a boundary-integral representation

$$\varphi(P) = \int_{S_B \cup S_S} [\varphi_n(Q)G(P, Q) - \varphi(Q)G_n(P, Q)]\mathrm{d}S(Q), \quad P \in \Omega \tag{2}$$

where $G(P, Q)$ is the free-space Green function for the Laplace operator, that is

$$G(P, Q) = \frac{1}{2\pi}\log(|P - Q|).$$

According to the governing equations (1), the velocity potential is assigned on the free surface, while its normal derivative is assigned on the body contour. The limit of the boundary-integral representation (2), as the point P approaches the boundary of the fluid domain, is taken, and a boundary-integral equation of mixed kind is obtained. Its solution provides unknown quantities along the body contour and the free surface.

The boundary-integral equation is numerically solved via a zero-order panel method. The velocity potential and its normal derivative are assumed to be constant along each panel and equal to the value they take at the centroid. In the discrete formulation, in addition to the body contour and the free surface, the domain Ω is also bounded by a far-field boundary S_F which is assumed to be circular. Since the far-field boundary is located at a finite distance from the main region, its contribution to the boundary-integral representation is not negligible and has to be taken into account. To evaluate this contribution it is assumed that, far from the body contour, the velocity potential approaches that of a vertical dipole [6]

$$C_D(t)\frac{y}{x^2+y^2} = C_D(t)\frac{\sin\theta}{r_F} = C_D(t)\varphi_D(x, y), \tag{3}$$

where r_F is the radius of S_F and the constant C_D is a function of time that has to be determined as a part of the solution. With the above considerations, for smooth contours the boundary-integral equation takes the form

$$\begin{aligned} &A(P) + \int_{S_B} \varphi(Q)G_n(P, Q)\mathrm{d}S(Q) - \int_{S_S\cup S_F} \varphi_n(Q)G(P, Q)\mathrm{d}S(Q) \\ &\qquad + C_D(t)\int_{S_F} \varphi_D(Q)G_n(P, Q)\mathrm{d}S(Q) = \\ &B(P) + \int_{S_B} \varphi_n(Q)G(P, Q)\mathrm{d}S(Q) - \int_{S_S} \varphi(Q)G_n(P, Q)\mathrm{d}S(Q), \\ &\qquad P \in S_B \cup S_S \cup S_F \end{aligned} \tag{4}$$

where

$$\begin{aligned} &A(P) = \frac{1}{2}\varphi(P), && B(P) = 0 && \text{for} \quad P \in S_B, \\ &A(P) = 0, && B(P) = -\frac{1}{2}\varphi(P) && \text{for} \quad P \in S_S, \\ &A(P) = \frac{1}{2}C_D(t)\varphi_D(P), && B(P) = 0 && \text{for} \quad P \in S_F. \end{aligned} \tag{5}$$

In order to determine C_D, an additional equation is introduced by requiring that the total incoming flow from the field boundary equals that provided by the dipole solution, that is,

$$-\int_{S_F} \varphi_n(Q)\mathrm{d}S(Q) + C_D(t)\int_{S_F} \varphi_{Dn}(Q)\mathrm{d}S(Q) = 0. \tag{6}$$

It is important to remark that, in Equation (4), the normal derivative of the velocity potential along the far-field boundary is not written as that of the dipole solution but, instead, is assumed to be a result of the boundary-integral equation. The resulting value of φ_n allows to compute the total flux through S_F and then, through Equation (6), to derive the constant of the dipole solution in an integral sense.

To discretize the solid contour, the shape of the impacting body is provided in terms of a cubic-spline representation passing through a given set of control points [12]. At each time step, the wetted portion of the body contour is first identified by using a linear extrapolation of the positions of the free-surface centroids and then discretized with straight line panels having their vertices located along the spline curve.

Once the linear system composed of the boundary-integral equation (4) and of the additional Equation (6) is solved, the normal derivative of the velocity potential on S_S, along with the tangential derivative φ_τ, completely determine the velocity field on the free surface, which is used to move the panel centroids. For stability reasons, the time step is chosen such that the maximum displacement of each centroid is always smaller than one fourth of the corresponding panel length. The dynamic boundary condition is also stepped in time to update the distribution of the velocity potential on the free surface. A cubic spline is passed through the new position of the panel centroids to reinitialize the position of the panel vertices. It is worth remarking that, although the boundary-integral equation (4) is numerically satisfied at the panel midpoints, Lagrangian markers used to track the free-surface motion are always lying along the spline curve, allowing a better conservation of mass [6].

The pressure distribution along the body contour is given by the Bernoulli equation

$$p = -\varrho_0 \left(\varphi_t + \frac{|\nabla\varphi|^2}{2} \right),$$

where ϱ_0 is the fluid density. The time derivative φ_t of the velocity potential might be computed numerically once the integral equation (4) has been solved. However, numerical differentiation is a source of errors and should be avoided if possible. In the present algorithm the boundary-value problem for the derivative φ_t is formulated and solved numerically. It exploits the fact that the derivative φ_t satisfies the Laplace equation in the flow domain Ω, the Dirichlet condition

$$\varphi_t = -\frac{|\nabla\varphi|^2}{2} \tag{7}$$

along the free surface, where the right-hand side is obtained from the solution of the integral equation (4), and the Neumann condition on the body contour [12]

$$(\varphi_n)_t = -w_\tau (u_n)_\tau + w_n (u_\tau)_\tau - k_\tau \boldsymbol{w} \cdot \boldsymbol{u} \tag{8}$$

where $\boldsymbol{w}$ and $\boldsymbol{u}$ denote the local velocity of the body and of the fluid and k_τ is the curvature of the body, which is negative for convex contours. The boundary-value problem for φ_t is similar to that for the velocity potential (1). Therefore, an integral equation similar to (4) can be derived for the time derivative φ_t. This integral equation is solved with the same technique as Equation (4), which provides the distribution of φ_t along the body contour.

The calculation is started by assuming that a very small portion of the body is already submerged and the velocity potential is null throughout the undisturbed free surface. The velocity field associated with these boundary conditions is singular about the intersection point and gives rise to a thin jet, characterized by very large velocities, that makes numerical modelling rather challenging. Indeed, the accurate description of the flow in this region needs a very fine resolution which, in turn, implies very small time steps in order to prevent numerical instabilities.

First attempts to deal with this complex flow, done by Yim [16] and Greenhow [13], showed that unphysical results can be obtained depending on the assumptions made about the intersection point. This problem has been overcome by Zhao and Faltinsen [6] who proposed to cut off from the computational domain the part of the jet where the angle between the free surface and the body contour is smaller than a threshold value. This part is replaced by a new panel, orthogonal to the body contour, along which a suitable boundary condition is applied.

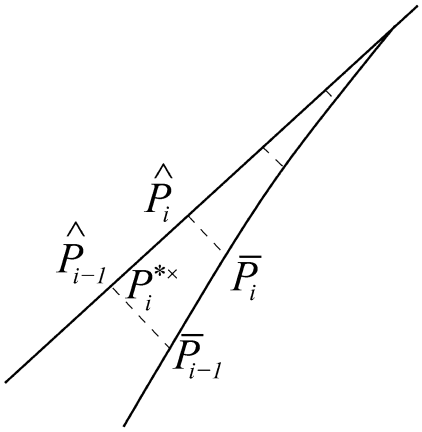

Figure 2. Definitions for the control volume V_i in the modelled part of the jet region.

Subsequently, a similar approach has been suggested by Fontaine and Cointe [17], with the cut criterion being based on the smallness of the local jet thickness.

The cut of the jet region is certainly reasonable when attention is mainly focused on the evaluation of the hydrodynamic loads, the pressure field inside the thin jet region being virtually negligible. As a matter of fact, models of this kind have been found to provide rather accurate predictions of the hydrodynamic loads experienced by impacting bodies of general shape [18, 12].

Nevertheless, such models have an intrinsic limitation in the procedure used to cut the jet. As an example, in the case of the impact with a constant entry velocity of two-dimensional wedges, the angle at which the cut is made cannot be smaller than the angle at the intersection point, as it is predicted from the similarity solution derived by Dobrovol'skaya [3]. While the limit angle is known for this rather simple configuration, analogous estimates are not available for arbitrary shapes of the impacting body or for arbitrary entry velocity. Furthermore, depending on the body shape and on the time history of the entry velocity, flow separation from the body contour can also take place. This is, for instance, the case of a circular cylinder, as it has been experimentally observed by Greenhow and Lin [19] and by Lin and Shieh [20].

In order to avoid the difficulties connected with the choice of a threshold condition beyond which to proceed to the cut of the jet, and in view of the development of a numerical approach able to deal with flow separation, a new model is proposed here which follows the thinner part of the jet with the help of a simplified representation of the velocity potential that is suitably matched with that in the bulk of the fluid.

2.2. Improved model for the jet region

When panel methods are used in the solution of boundary-integral equations, the accuracy of the solution cannot be guaranteed if the thickness of the computational domain is of the order of the panel size. As a consequence, an accurate description of the flow in the thin jet layer would require a very refined resolution which, in turn, implies small time steps to preserve the stability of the time-integration scheme. Furthermore, depending on the geometry of the impacting body, the angle at the jet tip can be rather small, and then a region always exists where the boundary-element approach fails, regardless of panel size.

The basic idea of the proposed model is to decompose the jet region into several small portions and, within each one, write the velocity potential as a local expansion truncated at a given order. The coefficients of the expansions are recovered by applying the boundary conditions on the body contour and on the free surface and by enforcing suitable matching conditions between adjacent portions. In spite of the different way used to approximate the velocity potential in the modelled part of the jet, the time-stepping procedure is just the same, as that used for the remaining part of the free surface. That is, the centroids of the free-surface panels are moved in a Lagrangian way and the velocity potential on them is updated correspondingly.

The modelled part of the jet is discretized into a number of fluid control volumes V_i. Each control volume is bounded on one side by the body contour and, on the opposite side, by the free surface (Figure 2). In order to make the enforcing of the boundary conditions easier, the four vertices of the control volume V_i are chosen as the centroids of the ith and $(i-1)$th panels on the body contour and the free surface. Inside V_i the velocity potential φ_i^J is written as a harmonic polynomial expansion about the midpoint P_i^*, that is

$$\begin{aligned}\varphi_i^J(x,y) = {} & A_i + B_i(x-x_i^*) + C_i(y-y_i^*) + \frac{D_i}{2}\left[(x-x_i^*)^2 - (y-y_i^*)^2\right] \\ & + E_i(x-x_i^*)(y-y_i^*).\end{aligned} \tag{9}$$

The coefficients of the expansion (9) are determined by applying the boundary condition at the four vertices of the control volume, that is,

$$\varphi_{in}^J(\hat{P}_{(i-1)}) = w_n(\hat{P}_{(i-1)}), \quad \varphi_{in}^J(\hat{P}_i) = w_n(\hat{P}_i), \tag{10}$$

$$\varphi_i^J(\bar{P}_{(i-1)}) = \varphi(\bar{P}_{(i-1)}), \quad \varphi_i^J(\bar{P}_i) = \varphi(\bar{P}_i), \tag{11}$$

where the terms on the right-hand side of Equations (11) are evaluated by integrating the dynamic boundary condition (7) with respect to time. A fifth condition is provided by the matching enforced with the adjacent control volume $V_{(i-1)}$. This matching condition can be formulated either as a continuity of the normal velocity on the free surface:

$$\varphi_{in}^J(\bar{P}_{(i-1)}) = \varphi_{(i-1)n}^J(\bar{P}_{(i-1)}), \tag{12}$$

or as a continuity of the velocity potential on the body contour:

$$\varphi_i^J(\hat{P}_{(i-1)}) = \varphi_{(i-1)}^J(\hat{P}_{(i-1)}). \tag{13}$$

In order to make smoother the transition between the bulk of the fluid and the modelled part of the jet, an intermediate region is interposed where the velocity potential is written as a weighted average of that given by the boundary-integral representation φ and that provided by the polynomial expansions φ^J:

$$\varphi^{\mathrm{av}}(P) = (1-l_i)\varphi(P) + l_i\varphi_i^J(P), \quad P \in V_i. \tag{14}$$

A limited number of control volumes are used inside this intermediate zone, with the weight function l_i linearly varying from zero, at the matching with the bulk domain, to unity, at the matching with the fully modelled zone. A similar average is applied to the matching conditions (12, 13) which become:

$$(1-l_i)\varphi_n(\bar{P}_{i-1}) + l_i\varphi_{in}^J(\bar{P}_{i-1}) = (1-l_{i-1})\varphi_n(\bar{P}_{i-1}) + l_{i-1}\varphi_{(i-1)n}^J(\bar{P}_{i-1}), \tag{15}$$

$$(1 - l_i)\varphi(\hat{P}_{i-1}) + l_i\varphi_i^J(\hat{P}_{i-1}) = (1 - l_{i-1})\varphi(\hat{P}_{i-1}) + l_{i-1}\varphi_{(i-1)}^J(\hat{P}_{i-1}). \tag{16}$$

Owing to the use of this jet model, the solution of the boundary-value problem is suitably modified in order to derive the coefficients of the expansions simultaneously. Hence, the discretized form of the boundary-integral equation (4) is used and it is coupled with the set of Equations (10, 11) and Equation (12) (or 13) written for the coefficients of the expansions in the control volumes. Furthermore, the weighted average (14) is used when writing the boundary-integral equation (4) in the intermediate region.

The unsteady contribution to the pressure field, φ_t, is derived by using an approach similar to that used to represent the velocity potential. Local expansions, similar to (9), are introduced along with a weighted average in the intermediate region. Then, a procedure completely similar to that used to derive the velocity potential is followed, allowing to recover the distribution of φ_t along the body contour and, hence, the pressure field.

A brief discussion is helpful to explain the criterion used to select the part of the jet along which the jet model is applied. At each iteration, starting from the tip, the local angle between the free surface and the body contour is evaluated and the point P^M on the free surface where this angle is large enough, say 30°, is identified. The modelled part of the jet is chosen as a fraction f_J, usually in the range 0·5–0·9, of the distance between the jet tip and the normal projection on the body contour of the point P^M. The extension of the intermediate region is a fraction f_I of the modelled part, and usually is of order $0{\cdot}3 f_J$.

As already stated, at each time step a cubic spline is passed through the panel centroids and the panel vertices are reinitialized to keep a good accuracy in the description of the flow in highly curved regions and in the jet zone. In particular, the panel distribution along the free surface in the bulk of the fluid is started from the matching point and a growth factor is used for the panel size. At the matching point the size of the first panel is assumed to be a fraction, about one-third, of the local jet thickness. The discretization of the modelled part of the jet into control volumes is carried out by using an analogous procedure.

3. Similarity solution for wedge impact

3.1. Formulation in self-similar variables

In order to validate the numerical model discussed so far, the similarity solution of the flow generated by the impact, with a constant entry velocity, of a two-dimensional wedge is derived here. The similarity solution for the wedge-entry problem has been already obtained by Dobrovol'skaya [3] in the form of a rather complicated nonlinear, singular, integral equation in terms of the free-surface slope. Owing to the behavior of this function at the jet tip, a very fine discretization and a quite sophisticated iterative procedure are needed for the solution of this problem, as shown by Zhao and Faltinsen [6].

In the present paper, the similarity solution is recovered by rewriting the governing equations in terms of self-similar variables. The boundary-value problem is solved with the help of a numerical approach similar to that employed in Iafrati and Korobkin [14] for the inner problem of the flow generated by a floating-wedge impact.

When the following set of self-similar variables

$$\xi = \frac{x}{Vt}, \quad \eta = \frac{y}{Vt}, \quad \phi = \frac{\varphi}{V^2 t}, \tag{17}$$

are introduced, the initial-boundary-value problem (1) takes the form:

$$\begin{aligned}
\phi_{\xi\xi} + \phi_{\eta\eta} &= 0 && \text{in} && \Omega^*, \\
\phi_\eta &= \phi_\xi \ \tan\alpha - 1 && \text{on} && S_B^*, \\
\phi + \frac{1}{2}|\nabla\phi|^2 &= \xi\phi_\xi + \eta\phi_\eta && \text{on} && S_S^*, \\
\nabla\phi \cdot \nabla H &= \xi H_\xi + \eta H_\eta && \text{on} && S_S^*, \\
\phi(\xi,\eta) &= O(1/\rho) && \text{for} && \rho \to \infty,
\end{aligned} \tag{18}$$

where $\rho = \sqrt{\xi^2 + \eta^2}$, $H(\xi, \eta) = 0$ is the equation of the free surface S_S^* in self-similar variables and Ω^* and S_B^* denote the fluid domain and the wetted-body contour, respectively.

Although independent of time, the boundary-value problem (18) is still made complicated by the boundary conditions on the free surface, the shape of which is unknown and has to be determined as a part of the solution. A significant simplification of the free-surface boundary conditions is obtained by introducing a modified velocity potential $S(\xi, \eta)$ as

$$S(\xi,\eta) = \phi(\xi,\eta) - \frac{1}{2}\rho^2 \tag{19}$$

from which

$$\phi_\xi = S_\xi + \xi, \qquad \phi_\eta = S_\eta + \eta. \tag{20}$$

When the above equations are used, the boundary condition on S_B^* takes the form

$$S_\eta + \eta = S_\xi \ \tan\alpha + \xi \ \tan\alpha - 1.$$

Since along the wedge surface $\eta - \xi \ \tan\alpha + 1 = 0$, the boundary condition along the body becomes

$$S_\eta = S_\xi \ \tan\alpha \quad \rightarrow \quad S_n = 0, \tag{21}$$

n being the normal to the fluid boundary, oriented inwards. In the same way, by inserting Equation (20) into the free surface boundary conditions, one obtains

$$\nabla S \cdot \nabla H = 0 \quad \rightarrow \quad S_n = 0 \tag{22}$$

for the kinematic condition and

$$S + \frac{1}{2}S_\tau^2 = 0, \tag{23}$$

for the dynamic one, τ being the parameter along the free surface which is zero at the intersection between the body contour and the free surface (Figure 3). In deriving Equation (23), the kinematic condition (22) is used to write $|\nabla S|^2 = S_n^2 + S_\tau^2 = S_\tau^2$. Finally, in terms of S, the far-field condition reads

$$S(\xi,\eta) \to -\frac{1}{2}\rho^2, \qquad \rho \to \infty. \tag{24}$$

The main advantage in using the modified velocity potential S is that the dynamic boundary condition on the free surface can be analytically integrated along it, thus yielding

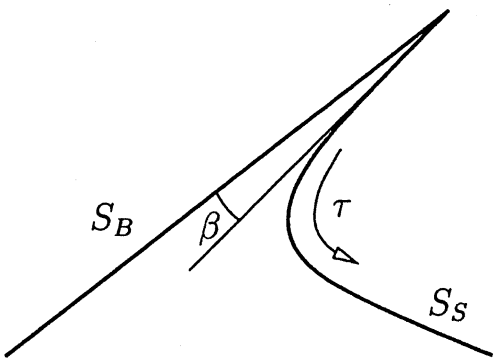

Figure 3. Sketch of the free surface configuration about the jet tip; τ is the curvilinear abscissa along the free surface with $\tau = 0$ at the tip.

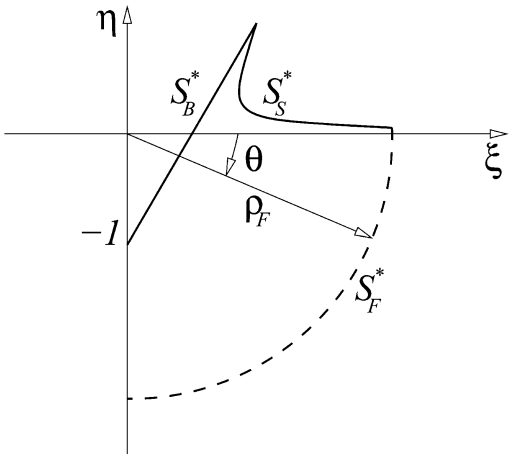

Figure 4. Sketch of the notation used when writing the problem in self-similar variables. Due to the symmetry, only the right hand side of the fluid domain is shown.

$$S(\tau) = -(\tau/\sqrt{2} + C)^2. \tag{25}$$

Let β denote the angle between the free surface and the body contour at the jet tip (Figure 3). In order to satisfy locally both the body boundary condition (21) and the kinematic condition (22), the constant C in Equation (25) has to be chosen such that

$$\lim_{\tau \to 0} S_\tau \ \sin \beta = 0$$

which, for $\beta \neq 0$, yields $C = 0$. Therefore, along the free surface

$$S(\tau) = -\frac{1}{2}\tau^2, \tag{26}$$

and, by using the definition (19), it follows that

$$\phi(\tau) = \frac{1}{2}(\rho^2 - \tau^2). \tag{27}$$

On the basis of the above considerations, the similarity solution is recovered by using the following iterative procedure. Starting from a first guess for the free surface shape S_S^*, the boundary-value problem

$$\begin{aligned} \Delta\phi &= 0 && \text{in} && \Omega^*, \\ \phi_n &= \cos\alpha && \text{on} && S_B^*, \\ \phi &= \tfrac{1}{2}(\rho^2 - \tau^2) && \text{on} && S_S^*, \\ \phi &\to 0 && \text{for} && \rho \to \infty \end{aligned} \tag{28}$$

is solved with the help of a boundary-integral representation of the velocity potential, thus providing the normal derivative of the velocity potential on the free surface which, by using the definition (19), allows to derive S_n as:

$$S_n = \phi_n - \boldsymbol{\rho} \cdot \boldsymbol{n} \tag{29}$$

and, hence, to check if the kinematic condition (22) is satisfied. If this is not the case, the free-surface configuration is updated, the velocity potential on it is reinitialized by using Equation (27) and the boundary-value problem (28) is solved once again. This iterative procedure is repeated until convergence is achieved. In the following, the numerical approach used to derive the similarity solution is discussed along with suitable procedures which are used in the far field and in the jet region to make the achievement of the convergence easier and faster.

3.2. NUMERICAL MODEL

The solution of the boundary-value problem (28) is numerically achieved with the help of a pseudo-time stepping approach which uses a boundary-integral representation of the velocity potential. At each point on the fluid boundary the velocity potential is written as

$$\frac{1}{2}\phi(P) = \int_{S_B^* \cup S_S^* \cup S_F^*} [\phi_n(Q)G(P, Q) - \phi(Q)G_n(P, Q)]\mathrm{d}S(Q), \tag{30}$$

where S_F^* is the far-field boundary of the computational domain, which is assumed to be of circular shape located at $\rho = \rho_F$.

According to the boundary-value problem (28), the velocity potential is assigned along the free surface and the far-field boundary, while its normal derivative is assigned on the body contour, thus obtaining

$$\begin{aligned} &\frac{1}{2}\phi(P) + \int_{S_B^*} \phi(Q)G_n(P, Q)\mathrm{d}S(Q) - \int_{S_S^* \cup S_F^*} \phi_n(Q)G(P, Q)\mathrm{d}S(Q) = \\ &\quad \int_{S_B^*} \phi_n(Q)G(P, Q)\mathrm{d}S(Q) - \int_{S_s^* \cup S_F^*} \phi(Q)G_n(P, Q)\mathrm{d}S(Q), \end{aligned} \tag{31}$$

which is numerically solved by a zero-order panel method. The boundary of the fluid domain is discretized with straight line panels along which a piecewise distribution is assumed for the velocity potential and for its normal derivative. By exploiting the symmetry with respect to the $\xi = 0$ axis, only the right-hand side of the fluid domain is discretized and the image contribution is accounted for when evaluating the influence coefficients (Figure 4). The velocity potential being assigned along S_S^* and S_F^* the first term on the left-hand side is moved into the right-hand side when Equation (31) is collocated on panels lying on free surface and far-field boundary.

As already stated, the iterative procedure is started from a first guess for the free-surface shape. From the solution of the boundary-value problem, the normal derivative of the velocity potential on the free surface is obtained, which, together with ϕ_τ, provides the velocity field. By use of Equation (29), S_n can be derived, thus allowing to check if the kinematic condition (22) is satisfied. The achievement of convergence is established in terms of the integral

$$\mathcal{K} = \int_{S_S^*} S_n^2 \mathrm{d}S.$$

Until convergence to the desired accuracy is reached, a new guess for the free-surface shape is obtained by stepping in time the solution by using

$$\nabla S = \nabla\phi - \boldsymbol{\rho} \tag{32}$$

as a pseudo-velocity field. Although it is not easy to prove that this choice actually leads to a convergent sequence free-surface configurations, numerical tests have shown that it naturally pushes the free surface towards the satisfaction of the kinematic constraint. As a matter of fact, once convergence is achieved, S_n is negligible, and reiterating the solution simply shifts the free-surface panels tangentially to themselves, thus leaving the free-surface shape substantially unchanged.

At each iteration the distribution of free-surface panels is reinitialized with new panel vertices located along a cubic spline passing through the centroids. The size of panels is suitably redistributed to preserve the accuracy in the description of the solution in the jet part and in highly curved regions. The reinitialization is started from the jet tip and the panel size progressively grows to fill the discretized part of the free surface.

Once the similarity solution is obtained, the pressure field along the body contour is evaluated from the unsteady Bernoulli equation which, in terms of self-similar variables, provides:

$$\frac{p}{\varrho_0 V^2} = -\phi + [\xi\phi_\xi + \eta\phi_\eta] - \frac{1}{2}\left[\phi_\tau^2 + \phi_n^2\right]. \tag{33}$$

and, in terms of tangential and normal derivatives, reads

$$\frac{p}{\varrho_0 V^2} = -\phi + \phi_\tau(\xi\ \cos\alpha + \eta\ \sin\alpha) + \phi_n\ \cos\alpha - \frac{1}{2}\left[\phi_\tau^2 + \phi_n^2\right].$$

If the condition $\phi = 0$ is enforced along the far-field boundary S_F^*, a very large value of ρ_F is needed to provide a solution which is independent of it. This limitation can be avoided by approximating the velocity potential with a dipole solution for $\rho \geq \rho_F$, as already done for the unsteady model. In this way a boundary-integral equation similar to Equation (4) is obtained with the dipole solution:

$$\phi_D = \frac{\sin\theta}{\rho_F},$$

Similar to what was done in Section 2.1, an additional equation is introduced for C_D, so that

$$-\int_{S_F^*} \phi_n(Q)\mathrm{d}S(Q) + C_D \int_{S_F^*} \phi_{Dn}(Q)\mathrm{d}S(Q) = 0. \tag{34}$$

Besides providing an improved boundary condition at the far field, thus allowing a significant reduction of the extension of the computational domain, the dipole solution enables also the derivation of an asymptotic estimate of the free-surface shape that can be used as an improved first guess from which the iterative procedure can be started. Actually, far from the jet region, the equation of the free surface can be presented in the form

$$H(\xi, \eta) = \eta - \zeta(\xi),$$

where $\zeta(\xi)$ is the free-surface elevation. The above equation, together with the kinematic boundary condition in (18), leads to

$$-\phi_\xi\zeta_\xi + \phi_\eta = -\xi\zeta_\xi + \zeta. \tag{35}$$

By using the dipole solution in Equation (35) and by neglecting higher-order terms, it follows

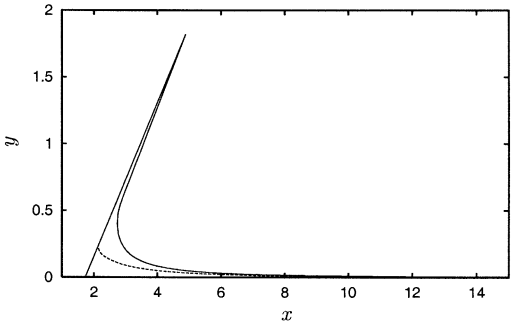

Figure 5. Comparison between the first free-surface guess obtained after the preliminar iterative cycle (*dashed line*) and the final self-similar solution obtained by using the model presented in Section 3. The calculation refers to a wedge with 30° deadrise angle.

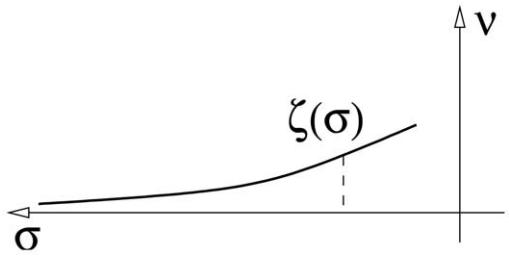

Figure 6. Local frame of reference introduced about the jet tip.

$$\frac{\mathrm{d}}{\mathrm{d}\xi}\left(\frac{\zeta}{\xi}\right) = -C_D \frac{1}{\xi^4},$$

that is,

$$\zeta(\xi) = \frac{C_D}{3\xi^2}. \tag{36}$$

Since the constant C_D is unknown at the beginning, only a few preliminary iterations are performed before starting the full iterative procedure. By assuming a flat free surface, the boundary-integral equation of the problem along with Equation (34) are solved, thus providing a first estimate of the constant C_D. This value allows the derivation of an improved free-surface guess through Equation (36) which is used as a new guess for the solution of the boundary-value problem, yielding a better estimate for C_D. Differently from the pseudo-time-stepping procedure, in these preliminar iterations free-surface changes are simply related to the different dipole constant C_D used in Equation (36). Usually four iterations provide a good estimate of the dipole coefficient C_D and of the free-surface shape. Concerning the latter point, in Figure 5 the first guess obtained after the preliminar iterative cycle is compared with the corresponding final solution of the problem for a wedge with 30° deadrise angle. It can be noted that the first guess is rather close to the final solution, but for a region very close to the jet root where, of course, the far-field asymptotics (36) is no longer valid.

3.3. Evaluation of the velocity field in the jet region

As already discussed, the boundary-element representation in the thin jet layer predicts an incorrect velocity field, the use of which for moving the free surface shape would produce an unphysical solution in the vicinity of the jet tip. In order to avoid this problem, an expansion of the velocity potential is written in terms of the local thickness of the jet. This expansion, matched with the solution provided by the boundary-element approach in a region where the thickness of the jet is small but still significantly larger than the local panel size, yields a new estimate for the velocity field on the free surface and of the velocity potential on the body contour in the thinner part of the jet.

In order to better explain this model, a local frame of reference is introduced, as shown in Figure 6. Within the jet region the velocity potential is approximated as

$$\phi(\sigma, \nu) = \tilde{\phi}(\sigma) + \cos\,\alpha(\nu - \zeta) + C_S(\nu^2 - \zeta^2), \tag{37}$$

which satisfies the boundary conditions on the body contour, $\nu = 0$, and on the free surface $\nu = \zeta(\sigma)$, since $\tilde{\phi}(\sigma) \equiv \phi(\sigma, \zeta(\sigma))$. The approximation (37) can be used if the angle at the jet tip is smaller than 45°, as it is for the wedge entry problem [3]. The constant C_S is recovered by enforcing the matching with the value of the velocity potential provided by the boundary-element solution for a point lying on the body surface just outside of the region where approximation (37) is used.

It has to be remarked that, when using expansion (37) to evaluate the velocity field, the continuity condition

$$(\phi_\sigma)_\sigma + (\phi_\nu)_\nu = 0$$

is not satisfied, that is the velocity field ϕ_σ, ϕ_ν obtained by a direct differentiation of Equation (37) is not that of an incompressible fluid. This problem is overcome by integrationg the Laplace equation in the normal direction from $\nu = 0$ to $\nu = \zeta(\sigma)$, thus obtaining

$$\frac{\mathrm{d}}{\mathrm{d}\sigma}\int_0^\zeta \phi_\sigma(\sigma, \nu)\mathrm{d}\nu - \zeta_\sigma\phi_\sigma(\sigma, \zeta) + \phi_\nu(\sigma, \zeta) - \phi_\nu(\sigma, 0) = 0.$$

Due to the impermeability constraint on the body contour, it follows that $\phi_\nu(\sigma, 0) = \phi_n = \cos\,\alpha$ and then

$$\frac{\partial\phi}{\partial\nu} = \cos\,\alpha + \zeta_\sigma\tilde{\phi}_\sigma - \frac{\mathrm{d}}{\mathrm{d}\sigma}\int_0^\zeta \phi_\sigma(\sigma, \nu)\mathrm{d}\nu, \tag{38}$$

which, by using Equation (37), provides

$$\frac{\partial\phi}{\partial\nu}(\sigma, \zeta) = \cos\,\alpha + \zeta_\sigma\tilde{\phi}_\sigma + \frac{\mathrm{d}}{\mathrm{d}\sigma}\left\{\zeta_\sigma\zeta\ \cos\,\alpha + 2C_S\zeta^2\zeta_\sigma - \tilde{\phi}_\sigma\zeta\right\}. \tag{39}$$

The above equation, along with the relation

$$\frac{\partial\phi}{\partial\sigma}(\sigma, \zeta) = \tilde{\phi}_\sigma - \cos\,\alpha\zeta_\sigma - 2C_S\zeta\zeta_\sigma, \tag{40}$$

completely describe the velocity field on the free surface, taking properly into account mass conservation. Hence, in the thin jet layer the pseudo-velocity field ($S_\sigma = \phi_\sigma - \sigma$, $S_\nu = \phi_\nu - \nu$) is used with ϕ_σ and ϕ_ν, evaluated from Equations (40) and (39), respectively.

In order to delimit the region where the jet model has to be employed, at each iteration, starting from the jet tip, the local angle between the free surface and the body contour is evaluated and the point P^M where the angle is large enough, say 30°, is identified. The jet model is used in a region ranging from the tip up to a fraction f_J of the distance between the jet tip and the normal projection onto the body contour of the point P^M. A substantial independence of the results of the value of f_J adopted is found, provided $f_J < 0{\cdot}7$.

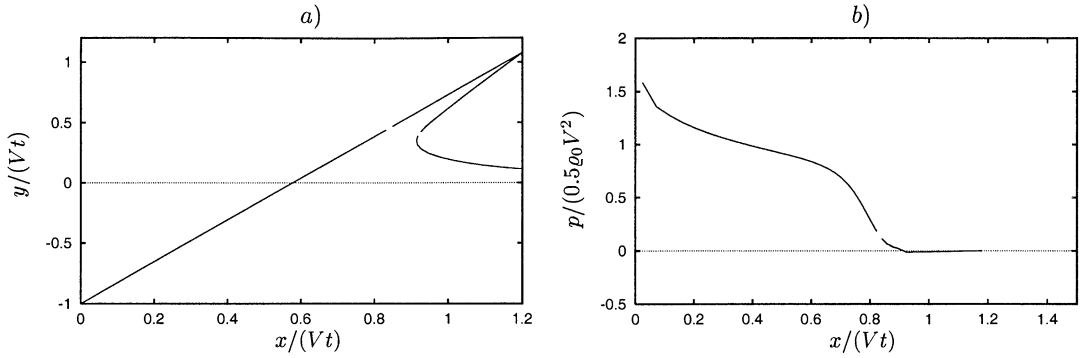

Figure 7. Comparison, in terms of free-surface shape (*a*) and pressure distribution (*b*), of results obtained by using the matching conditions (12) (*solid line*) and (13) (*dashed line*). The deadrise angle of the wedge is 60°.

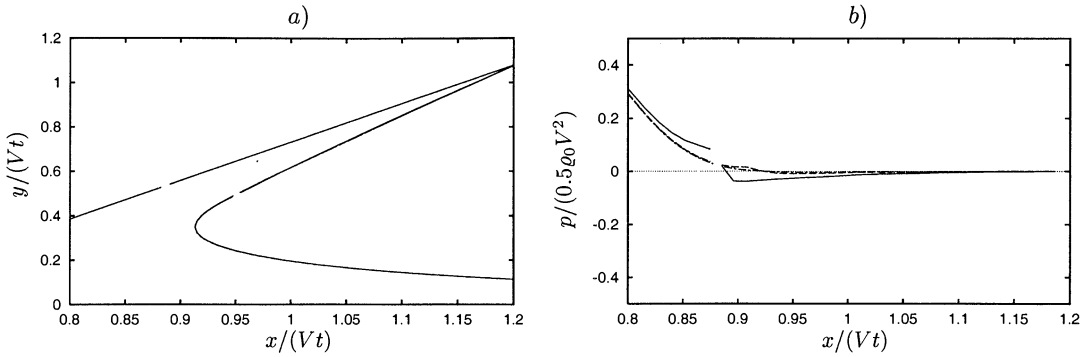

Figure 8. Effect of the extension of the intermediate region on the free-surface shape (*a*) and on pressure distribution (*b*). Three different values of f_I are used: 0 (*solid line*), $0{\cdot}25 f_J$ (*dashed line*) and $0{\cdot}5 f_J$ (*dash-dot line*). The deadrise angle of the wedge is 60°. In all the three cases the same fraction of the jet is modelled, $f_J = 0{\cdot}8$.

4. Numerical results

4.1. Verification of the proposed model

The numerical approach is used for computing the water impact, with constant entry velocity, of two-dimensional wedges having deadrise angles equal to 30° and 60°. Several computations are performed by using different values of the governing parameters and, in order to check the independence of the solution of them, comparisons are established in terms of free surface shape and pressure distribution. For the sake of clarity, all graphs are drawn in non-dimensional coordinates.

A first check aimed at evaluating which matching condition among control volumes performs better. In Figures 7*a*, *b*, two different solutions, obtained by using the matching conditions (12) and (13), are compared in the case of a wedge with 60° deadrise angle. No substantial differences occur in terms of free-surface shape and pressure distribution. Furthermore, a very mild transition is provided by both conditions, in spite of the rather large portion of the jet modelled, being $f_J = 0{\cdot}9$ and $f_I = 0{\cdot}35 f_J$. However, independently of the matching condition employed, a small negative pressure is predicted in a limited portion of the modelled jet region.

In order to achieve a better understanding of the motivation for this negative pressure, the role played by the modelled fraction, f_J, and by the extension of the intermediate region f_I,

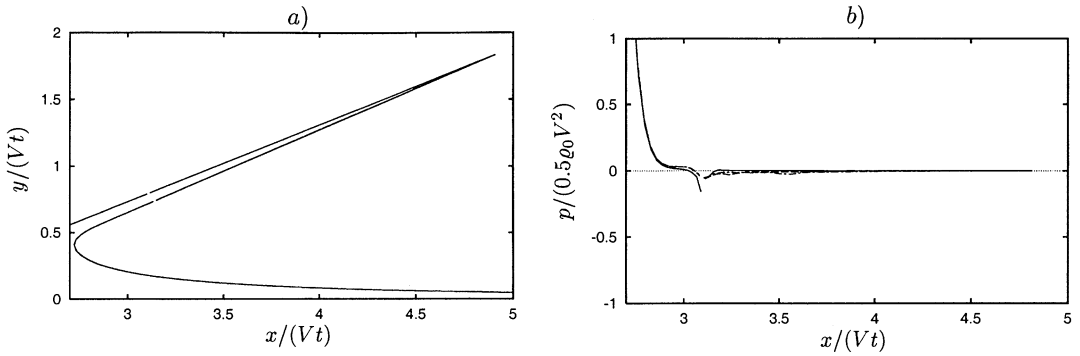

Figure 9. The same as in Figure 8 but the deadrise angle is 30°.

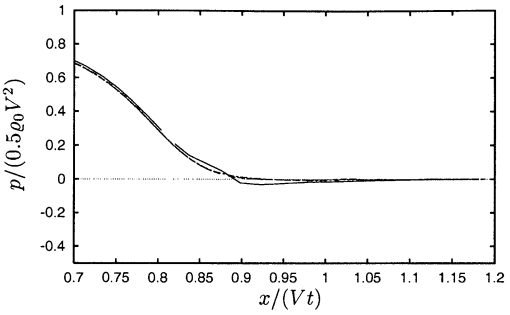

Figure 10. Effect of the extension of the modelled part of the jet on the pressure distribution. Three different values of f_J are used: 0·95 (*solid line*), 0·80 (*dashed line*) and 0·65 (*dash-dot line*). The deadrise angle of the wedge is 60°. In all the three cases the intermediate region has the same relative extension, $f_I = 0{\cdot}35 f_J$.

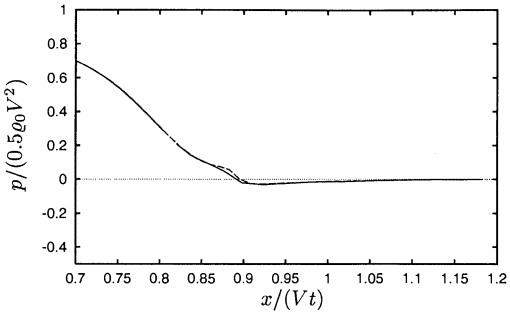

Figure 11. Effect of the resolution employed on pressure distribution. The same calculation, $f_J = 0{\cdot}95$, $f_I = 0{\cdot}35\, f_J$, is done by using panel size at the matching equals to 1/4 (*solid line*) and 1/8 (*dashed line*) of local the jet thickness.

is investigated. In Figures 8*a*, *b* and 9*a*, *b* enlarged views the transition region are depicted, showing the role played by f_I on wedges with 60° and 30° deadrise angle, respectively. Three different values of f_I are adopted, namely 0, $0{\cdot}25 f_J$, $0{\cdot}50 f_J$, while $f_J = 0{\cdot}8$ is used in all cases. Although the coefficient f_I does not have a visible influence on the free-surface shape, it is evident that the intermediate region cannot be too small if a smooth and regular transition in terms of pressure field is desired. For this reason, in the calculations $f_I = 0{\cdot}35 f_J$ is usually adopted.

With the aim of investigating the effects of f_J on the solution, three numerical calculations are performed in the 60° case by using different extensions of the modelled part, $f_J = 0{\cdot}95$, 0·8, 0·65, with $f_I = 0{\cdot}35 f_J$. In spite of the negligible effects found in terms of free-surface configuration (not shown here), the use of the model on a too wide region, say $f_J > 0{\cdot}8$, can lead to negative pressures inside the jet (Figure 10) which, as shown in the following, are not predicted by the similarity solution.

It is worth noting that, in the present numerical model, the fraction f_J indirectly assigns also the size of panels along the free surface, as is explained at the end of Section 2. The calculation shown in Figure 10 is obtained by using a panel size equal to one fourth of the

thickness of the jet at the root. In order to check if the wrong behavior of the pressure is related to the resolution employed, the calculation with $f_J = 0{\cdot}95$ is repeated by halving the panel size. Results, depicted in Figure 11, do not show a significant improvement of the solution, thus suggesting that, owing to the large jet thickness at the root for a modelled fraction as large as $f_J = 0{\cdot}95$, the local expansion (9) does not allow an accurate approximation of the solution.

All graphs presented above are drawn in terms of the non-dimensional variables, $x/(Vt)$, $y/(Vt)$ although the capability of the unsteady model to actually predict a similarity solution has not been proved yet. The latter point is investigated more deeply in the next section. In the following the constancy of the arc length between two fluid particles lying on the free surface, as demonstrated by Wagner [2], is checked. This test is carried out by choosing two fluid particles that, at the beginning of the impact, lie on the undisturbed free surface at a distance L_0. Then, during the penetration of the body, the location of the fluid particles on the free surface is identified and the actual distance L between them, as measured along the free surface, is calculated and its non-dimensional variation is evaluated as

$$L_v = \frac{L - L_0}{L_0}.$$

In addition to the constancy of the arc length, the accuracy of the numerical procedure is also evaluated in terms of mass conservation. With this aim, the area A^+, lying beneath the free surface in the half plane $y > 0$, and the area A^-, displaced by the body motion in the half plane $y < 0$, are computed and the non-dimensional mass variation is evaluated as

$$A_v = \frac{A^+ - A^-}{A^-}.$$

In Figure 12*a* the time histories of L_v and A_v are shown for a rather long time simulation, in the case of a wedge with 60° deadrise angle entering the water with a constant velocity $V = 1$. The results show that mass is very well conserved throughout the simulation, with largest variations, as small as 0·3 per cent, only occurring at the very beginning when the shape of the jet is still significantly changing.

A fairly satisfactory constancy of the arc length is also obtained, the largest variation being less that 0·5 per cent of the initial value. With respect to this point, it is worth noting that the initial location of the fluid particles is chosen so that, during the numerical simulation, they pass from the starting position, along the undisturbed free surface, until they are entirely inside the modelled part of the jet. This point can be seen by looking at the five free-surface configurations displayed in Figure 12*b*, along which the location of the fluid particles is marked by ticks, at instants of time corresponding to the ticks indicated along the curve for L_v in Figure 12*a*. The fact that for $t > 3{\cdot}5$ the arc is entirely lying inside the modelled part of the jet and that, up to the end of the simulation, variations of its length are bounded, demonstrates that the proposed model does actually predict a similarity solution with a good accuracy. In the next section the similarity solution obtained by a suitable scaling of the unsteady solution is compared with that provided by the solution of the self-similar problem discussed in Section 3.

4.2. Validation versus self-similar solution

The proposed jet model is found to be very stable and efficient. Due to the procedure used to discretize the modelled part of the jet region, the number of control volumes is not very

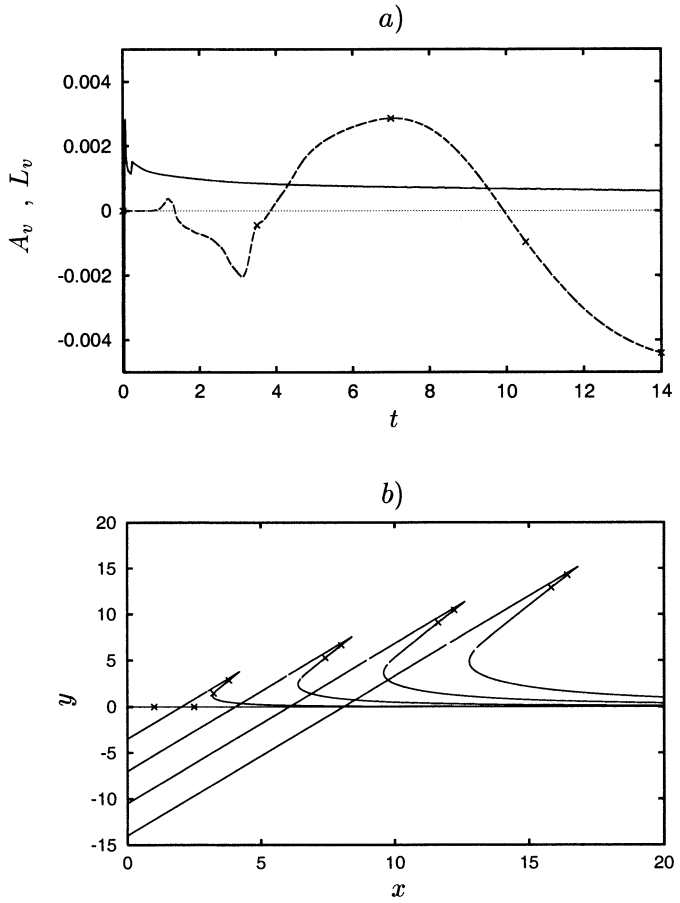

Figure 12. On (*a*) the relative variations of the area A_v (*solid line*) and of the arc length L_v (*dashed line*) are shown for a rather long numerical simulation of the unsteady water entry flow generated by a wedge with 60° deadrise angle. On (*b*), the free surface configurations along with the positions of the monitored arc (denoted by the ticks) are shown at five time instants ($t = 0, 3{\cdot}5, 7, 10{\cdot}5, 14$) corresponding to the ticks reported on the L_v curve in *a*.

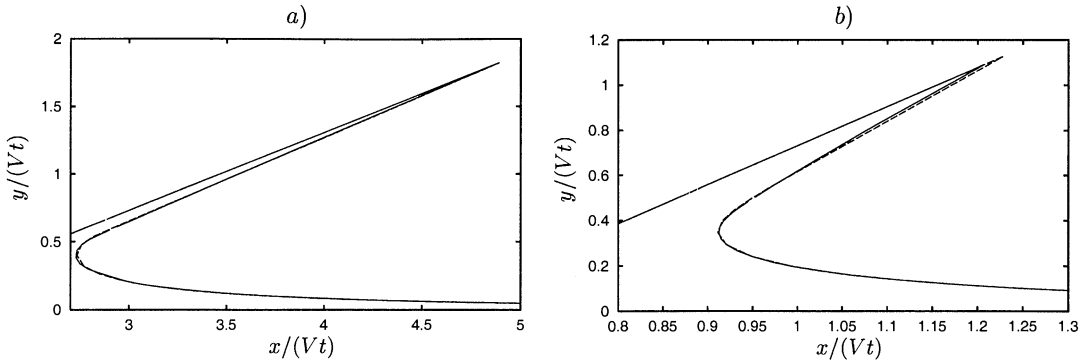

Figure 13. Comparison, in terms of free surface configuration, of the solution provided by the proposed model (*solid line*) and by the similarity model (*dashed line*) for the 30° (*a*) and 60° (*b*) case.

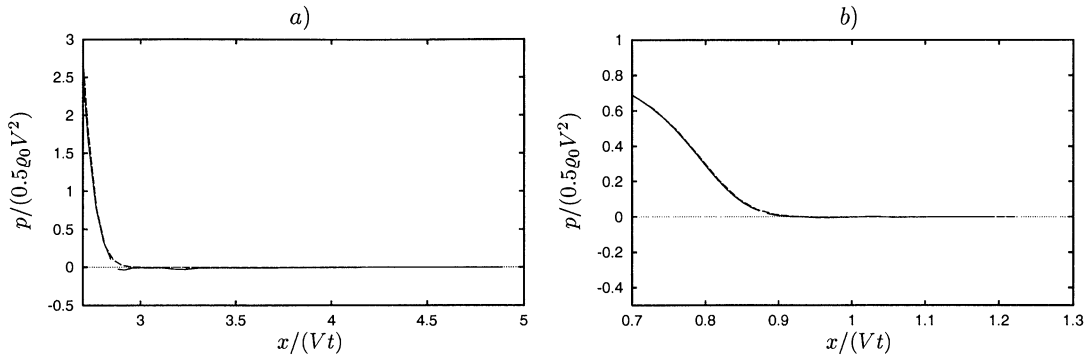

Figure 14. Comparison, in terms of pressure distribution, of the solution provided by the proposed model (*solid line*) and by the similarity model (*dashed line*) for the 30° (*a*) and 60° (*b*) case.

large and the additional complication of the linear system does not significantly increase the computational effort compared to the use of the cut model as done in [12].

In order to validate the proposed model comparisons are here established with the self-similar solution recovered with the formulation discussed in Section 3. In Figures 13*a*, *b* the comparison in terms of free-surface configurations is shown for wedges having deadrise angles of 30° and 60°, respectively. The agreement is satisfactory, although the wetted length predicted by the model for the 60° is slightly shorter than the self-similar one. In spite of this difference, a very good agreement is obtained near the jet root.

In Figures 14*a*, *b* the same comparison is presented in terms of pressure distributions. Attention being focused on the details of the solution in the jet region, only a close-up view about the transition region is shown. For the 60° case the agreement is definitively good, while a small disagreement occurs in the 30° case just at the first few elements of the modelled part.

As a final comparison, in Figures 15*a*, *b* the distributions of the velocity potential along the body contour and the free surface are shown. In both cases the agreement is quite good near the transition region, thus denoting a regular behavior of the velocity field in the jet region at the root of the modelled part. For the 60° case, a disagreement appears about the tip which is believed to be responsible for the shorter wetted length.

As a further validation of the proposed model, and of the similarity solution derived here as well, some relevant quantities are compared with the corresponding values recovered by Zhao and Faltinsen [6] by using the similarity solution of Dobrovol'skaya [3]. Results, reported in Table 1, confirm a good accuracy of the proposed model. A small discrepancy of the similarity solution derived here can be noticed in terms of the wetted length for the 60° case. Further investigations on this point are needed.

5. Concluding remarks

A simplified numerical model, capable of describing the unsteady free-surface flow and the pressure distribution taking place in the thin jet layer developing during water impact, has been presented. The model, conceptually based on a decomposition of the thin jet in small control volumes with local expansions approximating the distribution of the velocity potential, is incorporated into a boundary-element solver and the coefficients of the expansions are recovered together with the solution of the boundary-value problem. The proposed model, which exhibits good stability and accuracy properties, has been carefully analysed in order

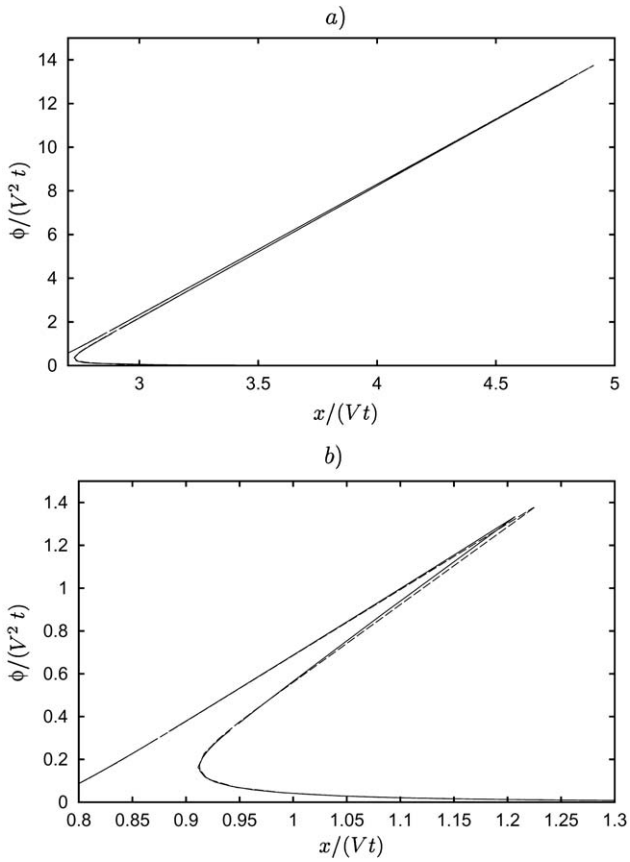

Figure 15. Comparison, in terms of velocity potential, of the solution provided by the proposed model (*solid line*) and by the similarity model (*dashed line*) for the 30° (*a*) and 60° (*b*) case.

to investigate the role played by the main parameters and a substantial independence of the results of them has been proved.

For the purpose of validation, the model has been applied to the unsteady flow generated by wedge impact, with constant entry velocity, and comparisons have been established with the corresponding similarity solution. The latter has been recovered through an iterative proced-

Table 1. Comparison of the tip elevation, $\eta_{\max}$, and the maximum pressure coefficient $C_{p\max} = p_{\max}/(0{\cdot}5\varrho_0 V^2)$ obtained by Zhao and Faltinsen [6] using the Dobrovol'skaya procedure (DOB) and the corresponding values provided by the similarity model here derived (SIM) and by the proposed numerical approach (NUM). Values are here shown for wedges with 30° and 60° deadrise angle

	$\eta_{\max}$ (60°)	$\eta_{\max}$ (30°)	$C_{p\max}$ (30°)
DOB	1·0848	1·8363	6·927
SIM	1·1263	1·8209	6·904
NUM	1·0908	1·8242	6·988

ure. Comparisons have shown that the proposed model provides fairly accurate predictions of the free-surface shape and of the pressure distribution along the wetted body contour. Furthermore, a very regular behavior of the solution has been found in the transition between the bulk of the fluid and the modelled part of the jet. The developed model is expected to be appropriate for dealing with separation effects.

Acknowledgements

The present research has been supported financially by the *Ministero dei Trasporti e Navigazione* in the framework of the INSEAN Research Plan 2000-02. The authors wish to thank Prof. A. Korobkin for the useful suggestions he gave them in developing the similarity model.

References

1. T. von Kármán, The impact of seaplane floats during landing. Technical Report TN 321. Washington: NACA (1929) 8pp.
2. H. Wagner, Über Stoß- und Gleitvorgänge and der Oberfläche von Flüssigkeiten. *Z. Angew. Math. Mech.* 12 (1932) 192–215.
3. Z.N. Dobrovol'skaya, On some problems of similarity flow of fluid with a free surface. *J. Fluid Mech.* 36 (1969) 805–829.
4. O.F. Hughes, Solution of the wedge entry problem by numerical conformal mapping. *J. Fluid Mech.* 56 (1972) 173–192.
5. N. de Divitiis and L.M. de Socio, Impact of floats on water. *J. Fluid Mech.* 471 (2002) 365–379.
6. R. Zhao and O.M. Faltinsen, Water entry of two-dimensional bodies. *J. Fluid Mech.* 246 (1993) 593–612.
7. R. Zhao, O.M. Faltinsen and J. Aarnes, Water entry of arbitrary two-dimensional sections with and without flow separation. In: E. Rood (ed.), *Proc. of 21st Symp. on Naval Hydrodynamics*. Trondheim: (1996) pp.118–132.
8. W. Vorus, A flat cylinder theory for vessel impact and steady planing resistance. *J. Ship Res.* 40 (1996) 89–106.
9. B.R. Savander, *Planing Hull Hydrodynamics*. PhD thesis. Dept. of Naval Architecture and Marine Engineering, University of Michigan (1997) 158pp.
10. L. Xu and A.W. Troesch, A study on hydrodynamics of asymmetric planing surfaces. In: SNAME (ed.), *Proc. of FAST '99.* Seattle: (1999) pp.471–481.
11. S. Muzaferjia, M. Peric, P. Sames and T. Schellin, A two-fluid Navier-Stokes solver to simulate water entry. In: E. Rood (ed.), *Proc. of the 22nd Symp. on Naval Hydrodynamics*. Washington (1998) pp.277–289.
12. D. Battistin and A. Iafrati, Hydrodynamic loads during water entry of two-dimensional and axisymmetric bodies. *J. Fluids Struct.* 17 (2003) 643–664.
13. M. Greenhow, Wedge entry into initially calm water. *Appl. Ocean Res.* 9 (1987) 214–223.
14. A. Iafrati and A.A. Korobkin, Starting flow generated by a floating wedge impact. Submitted for publication in *J. Engng. Math.* (2003).
15. M.S. Longuet-Higgins and E.D. Cokelet, The deformation of steep surface waves on water. I. a numerical method. *Proc. R. Soc. London* A350 (1976) 1–26.
16. B. Yim, Numerical solution of two-dimensional wedge slamming with a non linear free-surface condition. In: J.H. McCarthy (ed.), *Proc. of the 4th International Conference on Numerical Ship Hydrodynamics*. Washington (1985) pp.107–116.
17. E. Fontaine and R. Cointe, Asymptotic theories of incompressible water entry. In: *Proc. of AGARD FDP Workshop on High speed Body Motion in Water*. Kiev: (1997) pp. 25.1–25.9.
18. R. Zhao and O.M. Faltinsen, Water entry of arbitrary axisymmetric bodies with and without flow separation. In: E. Rood (ed.), *Proc. of 22nd Symp. on Naval Hydrodynamics*. Washington (1998) pp.652–664.
19. M. Greenhow and W.M. Lin, Non-linear free surface effects: experiments and theory. Technical Report 83-19. Boston: MIT, Dept. of Ocean Engineering (1983).
20. M.C. Lin and L.D. Shieh, Simultaneous measurements of water impact on a two-dimensional body. *Fluid Dyn. Res.* 19 (1997) 125–148.